Electric Power Systems Research 214 (2023) 108791

Contents lists available at ScienceDirect

Electric Power Systems Research

journal homepage: www.elsevier.com/locate/epsr

Accurate control of virtual oscillator-controlled islanded AC microgrids

Nabil Mohammed [a,*], Muhammad Ali [b], Mihai Ciobotaru [a], John Fletcher [b]

[a] School of Engineering, Macquarie University, Australia
[b] School of Electrical Engineering and Telecommunications, UNSW, Australia

ARTICLE INFO

Keywords:
Adaptive virtual impedance
Impedance measurement
Microgrid
Power sharing
Secondary control
VOC-based inverters

ABSTRACT

Virtual oscillator control (VOC) is an emerging control strategy for grid-forming inverters. In contrast with the droop and virtual synchronous generator methods, VOC is a nonlinear and time-domain strategy that requires only the inverter output current measurement to control the inverter output. Hence, it is characterized by its good dynamic response and stable operation. To explore the VOC performance in islanded AC microgrids, this paper initially demonstrates for the first time the negative impacts of impedance mismatching of the interfacing feeders on power sharing among VOC-based inverters. Then, new control schemes to enhance the operation of VOC-based islanded AC microgrids are proposed. First, a fast and robust secondary control loop to restore voltage and frequency in the microgrid based on the adaptive tuning of the VOC voltage-scaling factor and the VOC inductance parameters is developed. Second, an optimal tuning approach of virdual complex impedance combines virtual inductance and resistance for each inverter is proposed to fully mitigate the impacts of impedance mismatch of the interfacing feeders. Consequently, accurate active and reactive power sharing among VOC-based inverters is achieved. Third, an online and non-invasive estimation technique for feeder impedance is embedded in the control loop of each inverter. Hence, prior knowledge of feeders' impedances used to tune the virtual impedances of inverters is not required. Simulation and experimental results are presented to validate the efficacy of the proposed control scheme.

1. Introduction

With the recent remarkable development of power electronics technologies, the penetration level of distributed energy resources (DERs) units has increased significantly [1–4]. Clustering of DERs and loads as a single controllable system forms the concept of a microgrid that provides numerous benefits including the production of clean energy, expansion flexibility, and efficient and low-cost operation [5,6]. Most importantly, microgrids are resilient as they can operate in grid-connected and islanded mode. In islanded mode, the main tasks of inverter-based microgrids are to supply the load demand and to maintain the rated voltage and frequency [7,8].

In an inverter-dominant islanded AC microgrid mode as shown in Fig. 1, the droop control technique, which mimics the operation of synchronous generators in power plants, is usually embedded into the control loop of inverters. It enables reliable operation (e.g. self-regulation of units' output powers). However, the droop control technique inherently suffers from serious limitations related to the impedances of DG feeders. First, the conventional frequency–power droop control technique fails to achieve accurate power sharing among inverters [9]. It assumes pure inductive line impedance, whereas low voltage microgrids are mainly resistive with $R/X > 1$ [10]. Furthermore, the droop control has poor dynamic performance due to the use of low-pass filters in the control loop [11,12]. Second, the voltage drop across feeder impedances located between the inverters and load bus will cause deviations in the microgrid voltage at the load terminal from its desired nominal value. Therefore, improved control techniques should be adopted.

To enhance the accuracy of power sharing in droop-based islanded microgrids, improved droop-based control techniques have been proposed. Among these techniques, the virtual output impedance method has gained significant popularity. It is simple and capable to reshape the characteristics of the inverter output impedance. So, the coupling between the active and reactive power flow through feeders is minimized. Consequently, the power sharing accuracy among inverters is improved despite the impedance mismatch of the inverters feeders [12–14]. The implementation of virtual impedance could be complex resistive-inductive impedance [13], inductive [14], resistive [15], or complex resistive-capacitive impedance values [16]. Additionally, fixed [15, 17] and communication(less)-based adaptive values [12,14,18,19] for the virtual impedances have been investigated in the literature. To overcome voltage and frequency deviations challenge of droop-based islanded microgrids, secondary control was proposed in [11].

Virtual oscillator control (VOC) is an emerging control technique that was proposed recently to enable the decentralized operation of

* Corresponding author.
E-mail address: nabil.mohammed@ieee.org (N. Mohammed).

https://doi.org/10.1016/j.epsr.2022.108791
Received 21 April 2022; Received in revised form 30 July 2022; Accepted 4 September 2022
Available online 19 September 2022

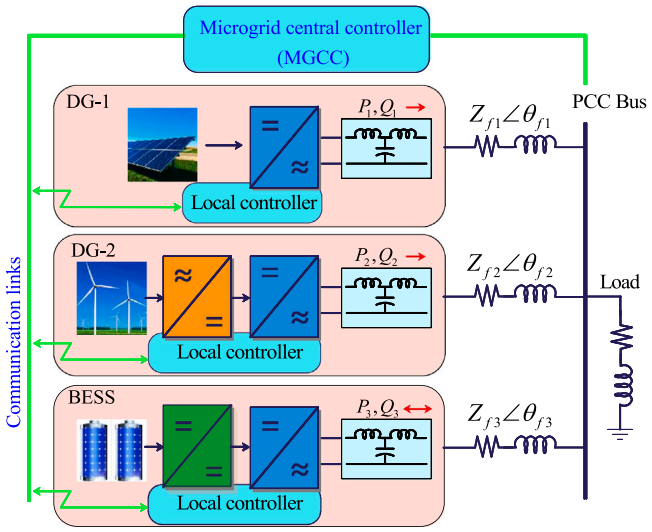

Fig. 1. Example of an inverter-dominant islanded AC microgrid.

inverter-based islanded AC microgrids. VOC regulates the inverter output power by emulating the nonlinear dynamics of a Van der Pol oscillator [20]. Similar to the classic droop control methods, VOC allows power sharing among parallel inverters. However, unlike droop control methods, VOC proves to provide better performance [21]. VOC is a time-domain controller that regulates the power flow based on the instantaneous current measurement only with no additional low pass filters. Hence, it provides a faster response during demand changes and transients compared to the droop control [20–22]. Given its advantages, VOC is appealing to researchers. [23] provided design guidance for VOC-based inverters operating in islanded mode. Synchronization of single- and three phase VOC-based inverters was proposed in [20,24], respectively. The virtual impedance technique was also embedded into the control loop of VOC-based inverters in [25,26].

To enable the operation of VOC-based inverters in grid-connected mode, improved VOC should be employed as power commands cannot be specified in the original VOC approach [3,20,24,27–30]. Therefore, dispatchable VOC (dVOC) were proposed in [27] to allow the regulation of active and reactive power, and it have been experimentally verified in [28]. In [29], a dVOC that relies on a complex-valued parameter for three-phase inverters connected to a nonstiff grid was presented. In [30], a secondary control loop to restore the microgrid voltage and frequency for islanded operation was also employed. Authors of [30,31] proposed methods to regulate the active and reactive output power of VOC-based inverters.

Summing up the above, despite current efforts to improve the overall performance of VOC-based islanded AC microgrids, several problems are mainly related to feeder impedances remain to be solved. First, the proposed secondary control loop in the literature to restore the microgrid voltage and frequency has slow dynamic response. It relies on the adaptive tuning of the VOC capacitance C and Voltage-scaling factor k_v. Second, to the authors' knowledge, neither an accurate power sharing strategy between VOC-based inverters that takes into account the impedance mismatch of feeders has been proposed nor the negative impacts of the impedance mismatch of feeders on the fair active and reactive power sharing between VOC-based inverters have been addressed. Addressing these key issues is necessary to ensure the reliable operation of VOC-based islanded AC microgrids. Finally, there is no existing approach in the literature addressing the optimal tuning of virtual impedances of the VOC-based inverters. This is important as the optimal procedure of assigning values to virtual impedance should consider the impedance mismatch of interfacing feeders to improve power sharing.

It is worth mentioning that the research community focuses recently on dispatchable VOC (dVOC) to solve certain limitations of the VOC based on Van-der-Pol type, such as the inherent 3rd harmonics and not being suitable for three phase systems. However, as the dVOC is only suitable for grid-connected mode or when it is desired to regulate the active and reactive power to their reference commands, in our paper the VOC based on Van-der-Pol is used as it is the only VOC based on Van-der-Pol type that allows self regulation of the frequency and voltage of the microgrid which is the core objective for reliable operation of islanded microgrids [11].

In this paper, an accurate control scheme for VOC-based islanded AC microgrid is proposed. The contributions of this paper are three folds:

1. Secondary control: a fast and robust secondary control loop for VOC-based islanded AC microgrid to maintain the rated voltage and frequency of the microgrid is proposed, which relies on adaptive tuning of the VOC inductance L and its voltage-scaling gain k_v.
2. Accurate power sharing: a new optimal tuning of the virtual complex impedance of each inverter based on the real mismatched values in the physical feeder impedances is proposed to ensure accurate active and reactive power sharing among VOC-based inverters.
3. Online impedance estimation: an online impedance estimation technique is embedded into the control loop of the VOC-based inverters. Hence, the prior knowledge of feeder impedances required to tune the virtual impedances is not needed.

This article is organized as follows: Section 2 reviews the operation concepts of VOC-based islanded microgrids including the encountered challenges related to the impedance mismatches of interfacing feeders. Section 3 illustrates the proposed control scheme (including the secondary control loop, virtual impedance, and online estimation of feeder impedances). Section 4 presents simulation results of a VOC-based islanded AC microgrid, followed by experimental results in Section 5. Finally, Section 5 concludes this article.

2. Operation of VOC for islanded microgrids

Fig. 2(a) shows the equivalent model of an islanded microgrid consisting of two single-phase inverters. Z_{f1} and Z_{f2} are feeder impedances containing R_{f1} and L_{f1} and R_{f2} and L_{f2}. Such islanded microgrid is required to (1) supply load demand, (2) share the load demand between inverters accurately and in proportion to their rated power, and (3) maintain the frequency and voltage of the microgrid equal to their nominal values. Therefore, reliable control such as droop control and VOC techniques shall be utilized. In this paper, the VOC control technique is considered due to its non-linear nature and fast response that leads to superior advantages compared to droop control.

Fig. 2(b) illustrates the implementation of the conventional virtual oscillator controller for a single-phase inverter. It can be observed that the control loop requires only the inverter output current measurement. The oscillator dynamics of the VOC-based inverter shown in Fig. 2(b) are described by the following nonlinear differential equations:

$$L\frac{di_L}{dt} = \frac{v}{k_v}. \tag{1}$$

$$C\frac{dv}{dt} = -\alpha\frac{v^3}{k_v^2} + \sigma v - k_v i_L + k_v k_i i. \tag{2}$$

where L and C are the virtual inductor and capacitance with a resonant frequency equal to the nominal system frequency (e.g., 50 Hz). σ is the virtual conductance. α is the cubic-current source constant. k_{v} and k_{i} are the voltage- and current-scaling factors that couple the virtual oscillator to the physical electrical system [20–24].

As this paper deals with low voltage microgrids that are dominantly resistive, VOC with embedded droop characteristics of $P-V$ and $Q-\omega$ is chosen for the remainder of this paper. The operation challenges due to feeder impedances of VOC-based islanded AC microgrids are illustrated in detail below.

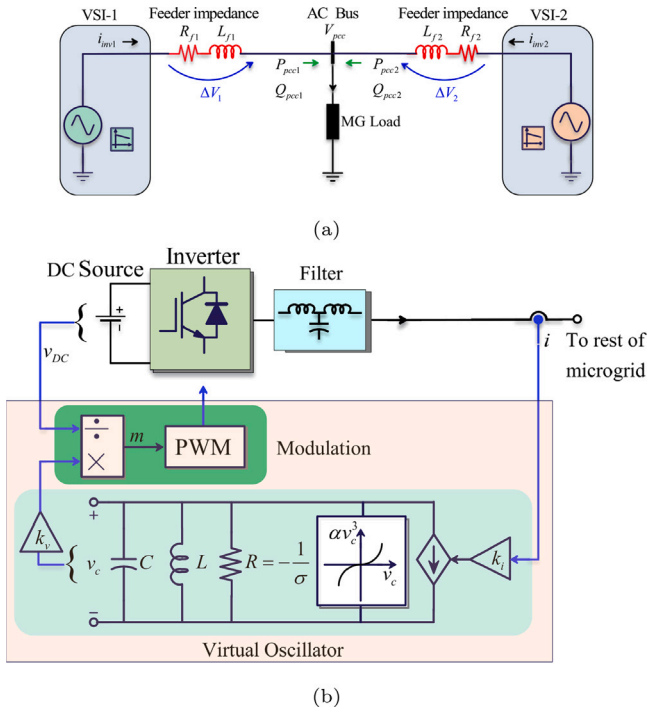

Fig. 2. (a) Equivalent schematic of two parallel inverters in an islanded microgrid (without virtual impedance), (b) Detailed implementation of virtual oscillator controller for single-phase inverter.

2.1. Voltage deviations

While adopting virtual oscillator control to control power inverters shows high-performance superiority, several challenges need to be fully addressed and solved. These problems are mainly related to the impedances of the main feeder and/or its branches in the islanded AC microgrids. First, VOC-based inverters act like voltage sources. They control the voltage and frequency of the microgrid. However, the microgrid voltage and frequency deviate from their nominal values. The main cause of these deviations is related to voltage drops across feeder impedances.

For the equivalent model of microgrid shown in Fig. 2(a), the voltage drop across impedance of feeder k is calculated as follows:

$$\Delta V_k \approx \frac{X_{fk}Q_k + R_{fk}P_k}{E^*}. \tag{3}$$

where P_k and Q_k are active and reactive power flow in feeder k (k= 1, 2). R_{fk} and X_{fk} are the resistance and inductance of the same feeder. E^* is the nominal voltage.

Therefore, the voltage drop expressed in (3) will result in deviations of the PCC voltage (also called in this paper as microgrid/load voltage) from the nominal value, whether the impedance of feeder 1 (Z_{f1} = R_{f1}+ jX_{f1}) and the impedance of feeder 2 (Z_{f2} = R_{f2}+ jX_{f2}) are equal or not. Therefore, secondary control loop should be utilized to restore the microgrid voltage and frequency.

2.2. Disproportion active and reactive power sharing among VOC-based inverters

If the two inverters shown in Fig. 2(a) are identical, then, both inverters will share the load active ,and reactive power equally only if the impedances of their feeders are equal. Z_{f1} = Z_{f2}. Otherwise, the shared power will be disproportionate among these VOC-based inverters. To further illustrate, if Z_{f1} is assumed to be larger that Z_{f2}, then, mismatched resistance and inductance between the two feeders are expressed as follows:

$$\begin{cases} \Delta R_f = R_{f1} - R_{f2} \\ \Delta X_f = X_{f1} - X_{f2}. \end{cases} \tag{4}$$

Consequently, the mismatched voltage drop (δV) across the mismatched impedances of feeder 1 and feeder 2 shown in (4) is expressed as:

$$\delta V_1 = f(\Delta R_f, \Delta X_f). \tag{5}$$

Despite both VOC-based inverters being identical, the voltage drop across the non-equal impedances of the two feeders causes inaccurate active and reactive power sharing between the two inverters. For the resistive VOC (with $P-V$ and $Q-\omega$ droop characteristics), it is found that Inverter 1 supplies less active power, than Inverter 2, $P_{pcc1} < P_{pcc2}$. In contrast, Inverter 2 supplies more reactive power for the same test conditions, $Q_{pcc1} > Q_{pcc2}$. The overall effects of impedance mismatch of interfacing feeders on both the active and reactive power sharing among VOC-based inverters are summarized in (6).

$$\begin{cases} Z_{f1} > Z_{f2} \\ \Delta V_1 > \Delta V_2 \\ P_{pcc1} < P_{pcc2} \\ Q_{pcc1} > Q_{pcc2}. \end{cases} \tag{6}$$

3. The proposed control for virtual oscillator based islanded AC microgrids

The proposed control scheme for VOC-based islanded AC microgrids, which is consisting of secondary control, virtual impedances, and online impedance estimation of DG feeders, is elaborated below.

3.1. Proposed secondary control based on adaptive tuning of VOC parameters

The microgrid is inherently subject to frequency and voltage deviations ($\delta\omega$, δV). Hence, an external secondary controller is employed to eliminate these deviations. This proposed approach is summarized in (7) and (8). It relies on the adaptive tuning of the nominal VOC parameters (L_0, k_{v_0}) based on the deviations in the microgrid frequency (ω_{MG}) and RMS voltage (V_{MG}) processed in the secondary loop.

$$L = \underbrace{L_0}_{\text{fixed}} + \underbrace{(K_p^{\omega} + \frac{K_i^{\omega}}{s})(\omega_{MG}^* - \omega_{MG})}_{\text{adaptive } (\delta\omega)} \tag{7}$$

$$k_v = \underbrace{k_{v_0}}_{\text{fixed}} + \underbrace{(K_p^{v} + \frac{K_i^{v}}{s})(V_{MG}^* - V_{MG})}_{\text{adaptive } (\delta V)} \tag{8}$$

Where K_p^{ω}, K_i^{ω}, K_p^{v} and K_i^{v} are the parameters of secondary control. The control scheme of the microgrid is presented in detail in Fig. 3. The low bandwidth communications, shown in green color, were employed for (1) implementation of the external secondary control [11], and (2) estimation of feeder impedances, and (3) broadcasting the estimated impedance information of feeder 1 ($\hat{R}_{f1}$, $\hat{L}_{f1}$) to the other inverter(s).

3.2. Proposed virtual impedance for accurate active and reactive power sharing

It was demonstrated in (6) that the impedance mismatch of the feeders will result in unfair active and reactive power sharing, where some VOC-based inverters will supply more active or reactive power than others. To mitigate such negative impacts, an optimal tuning of virtual impedance (Z_v) is proposed in this paper. The core idea of

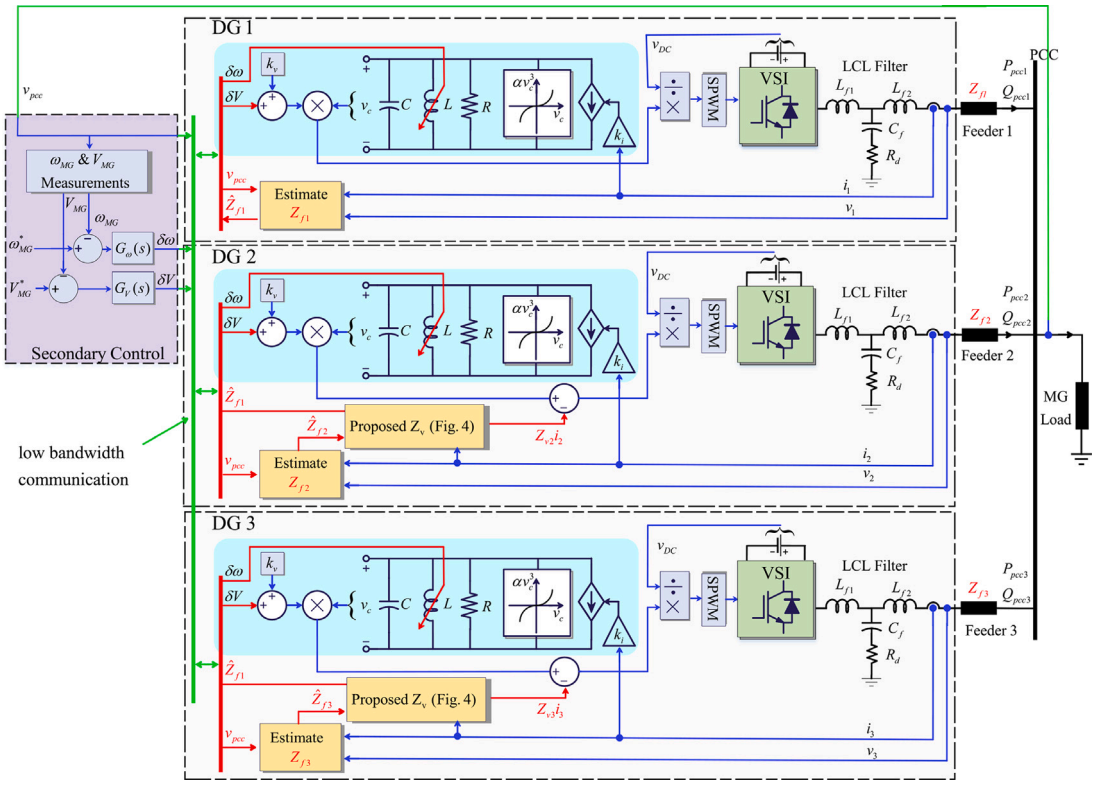

Fig. 3. Proposed secondary control and virtual impedance loops for VOC-based inverters in islanded mode to achieve (1) frequency and voltage regulation, and (2) accurate active and reactive power control, respectively.

virtual impedance is to modify the output impedance of a given inverter as follows:

$$v_k^* = v_{refk} - Z_{vk} i_k. \tag{9}$$

Where v_k^* and v_{refk} denote the dropped voltage reference and the voltage reference for inverter k, respectively. i_k is the inverter output current. $Z_{vk} = R_{vk} + jX_{vk}$ is the virtual impedance assigned to the k^{th} inverter. However, the remaining challenge is to determine the optimal value of Z_v assigned to each inverter.

The proposed approach relies on calculating the impedance mismatch of the DG feeders to determine the optimal values of virtual complex impedance for each inverter. The tuning procedure of the virtual impedances takes into account the complex impedances of all feeders (resistive and inductive parts).

Therefore, the impedance information on each feeder should be known. It can be obtained by either having prior knowledge (design/cable specifications) or using an online impedance estimation technique. In this paper, the second approach is considered as will be explained in the next subjection. The control laws of the proposed optimal tuning of the virtual impedances for the AC microgrid consisting of 1 ... k^{th} inverters are expressed as follows:

$$\begin{cases} Z_{v1} = 0 \\ Z_{v2} = (\hat{Z}_{f1} - \hat{Z}_{f2}) \\ \dots \\ Z_{vk} = (\hat{Z}_{f1} - \hat{Z}_{fk}). \end{cases} \tag{10}$$

where Z_{v1}, $Z_{v2} = R_{v2} + jX_{v2}$, $Z_{v3} = R_{v3} + jX_{v3}$ and $Z_{vk} = R_{vk} + jX_{vk}$ are the proposed virtual impedances for inverters 1, 2, ... k^{th}, respectively. $\hat{Z}_{f1} = \hat{R}_{f1} + j\hat{X}_{f1}$, $\hat{Z}_{f2} = \hat{R}_{f2} + j\hat{X}_{f2}$ and $\hat{Z}_{fk} = \hat{R}_{fk} + j\hat{X}_{fk}$ are the estimated impedances in real-time of feeders 1, 2 and k, respectively.

To further explain the followed methodology for online tuning of the virtual impedances, the inverter-based microgrid shown in Fig. 3 is investigated. First, inverters 1, 2, and 3 online estimate the impedances of feeders 1, 2 and 3, respectively. Then, inverter 1 is taken as the base case, where its virtual impedance is set to zero. Simultaneously, the estimated impedance of feeder 1 is broadcast to the other inverters. Third, the virtual impedances of these inverters are set according to the difference between the estimated impedances of their feeders and the shared impedance information of feeder 1. Finally, $Z_{v2} i_2$ and $Z_{v3} i_3$ are subtracted to modify the voltage references according to (9).

As a result, the mismatched feeder impedances presented in (4) are compensated online in the control loop of the inverters. Hence, mismatched voltage drops calculated in (5) across feeders are being fully mitigated. Consequently, fair active and reactive power sharing among VOC-based inverters is ensured. The power sharing performance after enabling the proposed virtual impedances under impedance mismatch of the inverters feeders is summarized in (11).

$$\begin{cases} \Delta V_1 = \Delta V_2 \dots = \Delta V_k \\ (Z_{f1} + Z_{v1}) i_1 = (Z_{f2} + Z_{v2}) i_2 \dots = (Z_{fk} + Z_{vk}) i_k \\ P_{inv1} \cong P_{inv2} \dots \cong P_{invk} \\ Q_{inv1} \cong Q_{inv2} \dots \cong Q_{invk}. \end{cases} \tag{11}$$

Where ΔV_k, is the voltage droop see by the k^{th} inverter and Z_{fk} is the physical impedances of feeder k^{th}.

Fig. 4 presents in detail the implementation of the proposed virtual impedance for the k^{th} inverter. The estimated impedance and the second-order generalized integrator (SOGI) are utilized to facilitate the real-time implementation [13]. It is worth mentioning that proposed virtual impedances do not need to be tuned again as their values depend only on the physical impedances of the microgrid feeders. This advantage makes the proposed virtual impedance control scheme tolerant of communication disruptions/delays. So, the continuous estimation of the feeder impedances is not required as long as the feeder impedances remain constant.

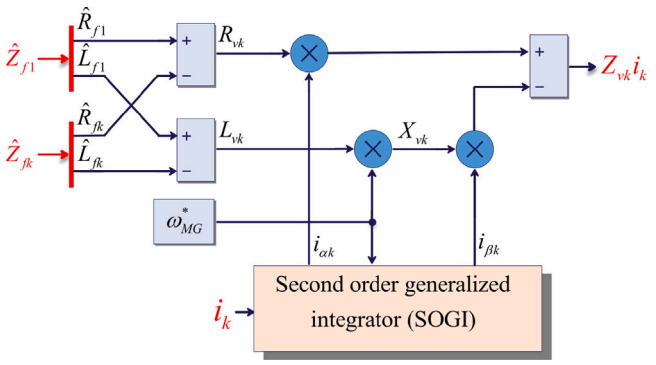

Fig. 4. Implementation of the proposed virtual complex impedance for the kth inverter.

3.3. Online estimation of feeder impedances

As stated earlier, the impedance of a particular interfacing feeder is estimated online by the inverter located at the end of that feeder. For instance, Inverter 1 estimates the impedance of feeder 1 and so on with other inverters. For the estimation purposes, this paper utilizes an online non-invasive estimation based on the recursive least squares (RLS) algorithm [32] that is implemented in the control loop of each inverter, as shown in Fig. 3.

To further elaborate, the impedance estimation procedure of feeder 1 by using the RLS algorithm implemented into the control loop of Inverter 1 is explained below. First, the steady state operation of inverter 1 can be described as follows:

$$v_1 = R_{f1} \times i_1 + L_{f1} \times \frac{di_1}{dt} + v_{pcc}. \tag{12}$$

Where v_1 and i_1 are the instantaneous inverter output voltage and current measurements, respectively. v_{pcc} is the microgrid (load) voltage. Then, v_1 and v_{pcc} are chosen as the system input variables, and i_1 is chosen as the state variable. Finally, the continuous-time state space model is discretized and rearranged in linear regression form as expressed in (13).

$$i_1(k) = \begin{bmatrix} i_1(k-1) \\ v_1(k-1) - v_{pcc}(k-1) \end{bmatrix}^T \begin{bmatrix} 1 - \frac{R_{f1}}{L_{f1}} T_s \\ \frac{1}{L_{f1}} T_s \end{bmatrix}. \tag{13}$$

where T_s is the sampling interval of the inverter controller. Now, the values of R_{f1} and L_{f1} are calculated online using the RLS algorithm based on the three measurement quantities (v_1, i_1 and v_{pcc}).

Based on (13), the linear regression is established as expressed in (14).

$$y(k) = \varphi^T(k) \times \theta \tag{14}$$

Where $y(k)$ is the output vector. $\varphi^T(k)$ is the vector that includes input sampled voltage and current variables. θ is the regression vector of the unknown impedance components of feeder 1 (R_{f1}, L_{f1}).

A similar analysis is followed for the online impedance estimation of feeder 2 and feeder 3 by inverter 2 and inverter 3, respectively.

4. Simulation results

To validate the performance of the proposed control strategy, an islanded microgrid consisting of three single-phase inverters shown in Fig. 3 is considered. The system and control parameters are listed in Table 1. The system is simulated in MATLAB/Simulink software, where different scenarios are investigated. These scenarios are to test the performance of the proposed control scheme under impedance mismatched of the feeders and to evaluate the reliability of the proposed power sharing strategy considering communication delays/failure.

Table 1
System and control parameters.

Quantity	Symbol	Value	Unit
Microgrid parameters			
Nominal voltage (RMS)	V^*_{MG}	230	V
Nominal frequency	ω^*_{MG}	2π 50	rad/sec
Initial load power	$P_{load\ ref1}$	9	kW
	$Q_{load\ ref1}$	6	kVar
Final load power	$P_{load\ ref2}$	6	kW
	$Q_{load\ ref2}$	4.5	kVar
R/X ratio of feeders 1,2,3	R/X	9.435	Ω/Ω
Impedance of feeder 1	R_{f1}	0.868	Ω
	L_{f1}	0.29285	mH
Impedance of feeder 2	R_{f2}	0.434	Ω
	L_{f2}	0.1464	mH
Impedance of feeder 3	R_{f3}	0.217	Ω
	L_{f3}	0.0732	mH
DG1, DG2 and DG3 circuit parameters			
Inverter nominal active power	P_n	5	kW
Inverter nominal reactive power	Q_n	5	kVar
Filter inverter-side inductance	L_1	2.5	mH
Filter grid-side inductance	L_2	0.9748	mH
Filter capacitance	C_f	4.7	uF
Damping resistance	R_d	3.3	Ω
DG1, DG2 and DG3 VOC parameters (Primary Control)			
Current-scaling factor	k_i	0.0432	A/A
Voltage-scaling factor	k_{v_0}	253	V/V
Conductance	σ	4.3381	Ω^{-1}
Cubic-current source coefficient	α	2.8921	A/V^3
Oscillator inductance	L_0	54.415	uH
Oscillator capacitance	C	0.1862	F
Switching frequency	f_{sw}	10	kHz
Secondary control			
Frequency restoration gains	K^{ω}_p	10^{-7}	–
	K^{ω}_i	10^{-6}	1/s
Voltage restoration gains	K^{v}_p	0.1	–
	K^{v}_i	10	1/s

4.1. Performance of the proposed control scheme under impedance mismatched of the feeders

Five different scenarios are investigated to test the performances of the (1) the conventional primary VOC control ($t < 3$ s), (2) the proposed secondary control ($t \geq 3$ s), (3) the proposed virtual impedance ($t \geq 6$ s), (4) step-change in the microgrid active load ($t \geq 9$ s), and finally, (5) step-change in the microgrid reactive load ($t \geq 12$ s).

Fig. 5(a) and Fig. 5(b) present the microgrid active and reactive load. It can be seen that the delivered power to the load is less than the desired references under the conventional primary VOC control. For instance, the delivered active and reactive power to the load is around 8 kW and 5.35 kVar for $t < 3$ s, where the desired references are $P_{load\ ref1}$= 9 kW and $Q_{load\ ref1}$= 6 kVar, respectively. It is worth mentioning that the given power references in Fig. 5 are the active and reactive power references of the microgrid load and they were calculated at the nominal conditions (230 V, 50 Hz). After the activation of the proposed secondary control for $t \geq 3$ s, the errors in both the active and reactive power are regulated to zero even after load changes at t= 9 s and t= 12 s

Fig. 6(a) and Fig. 6(b) show the shared active and reactive power of the three VOC-based inverters. It can be observed that the VOC control failed to share the microgrid load accurately among the inverters for $t < 6$ s under mismatched feeder impedances, even after the enabling of the proposed secondary control for t= [3–6] sec. For example, Inverter 1 supplied less active power and more reactive power compared to other inverters as it has the smallest feeder impedance. For $t \geq 6$ s, Inverters 1, 2, and 3 share the same amount of active and reactive power under the proposed virtual impedance. It can be seen that the reactive power in Fig. 5(b) and Fig. 6(b) have significant overshoot or

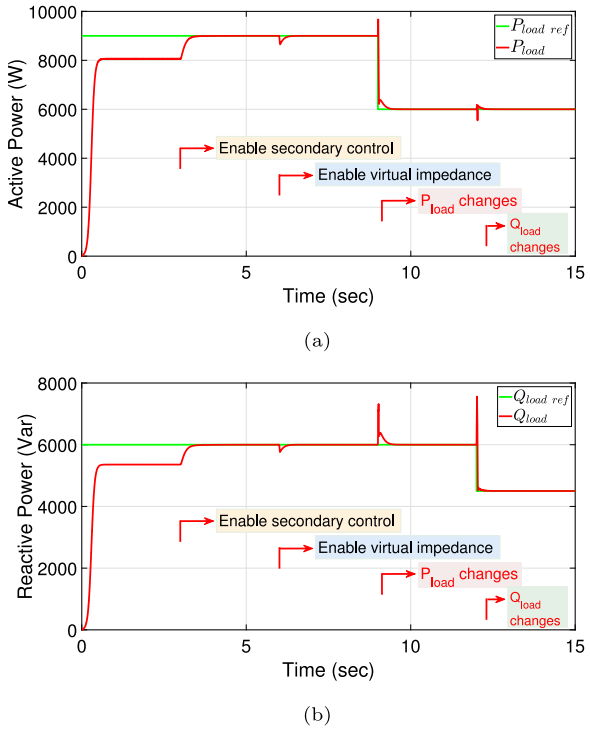

Fig. 5. Active and reactive power of the microgrid load.

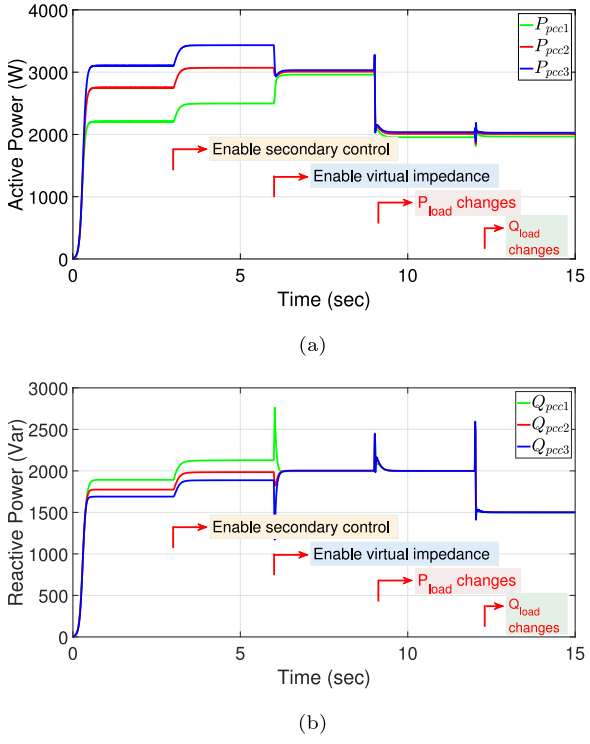

Fig. 6. Load power sharing among the three inverters: (a) Active power and (a) Reactive power.

undershoot indicating that the reactive power flow is much sensitive to the sudden changes of the VOC parameters.

Fig. 7 depicts the waveforms of inverters output currents, i_{inv1}, i_{inv2}, and i_{inv3}. Additionally, the load current i_{load} is depicted in the same figure. The zoomed-in zero-crossing instants show that initially the magnitude and phase of inverters output currents are not identical. In

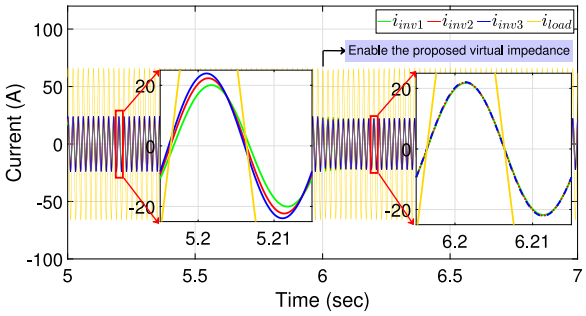

Fig. 7. Microgrid currents waveforms.

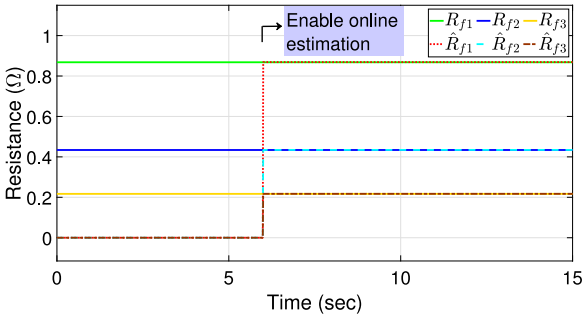

Fig. 8. Online resistance estimation of feeder 1, 2, and 3 by Inverter 2, 3, and 3, respectively.

contrast, the magnitude and phase of these currents are matching under the proposed virtual impedance enabled for $t \geq 6$ s

Fig. 8 shows the estimated resistances of feeder 1, 2, and 3 by Inverter 1, 2, and 3, respectively. Compared to the reference values listed in Table 1, it can be observed that the obtained estimation results by the RLS algorithm are very accurate.

Fig. 9(a) shows the RMS voltages in the microgrid. It can be observed that the secondary control regulated the microgrid voltage V_{MG} to its nominal value of 230 V, where it was 217.5 V for $t < 3$ s Fig. 9(a) indicates that the terminal RMS voltage of Inverter 1 (V_{inv1}) has the highest value compared to the voltages of other inverters. This is true as the voltage drop across the impedances of feeder 1 will be greater than the voltage drops across impedances of feeders 2 and 3. Fig. 9(b) shows the restoration of microgrid frequency from 50.2 Hz to its nominal value of 50 Hz. Fig. 9(a) and Fig. 9(b) indicate the fast response of the proposed secondary control loop to regulated the frequency and voltage, around 0.5 s and 1.5 s, respectively. These time instants based on varying the VOC inductance were much smaller compared to the reported response times (14.5 s and 40 s) of the secondary control presented in [30] which relied on varying the VOC capacitance.

4.2. *Lose of communication*

A key concern in microgrid operations is to evaluate the impact of the communication failure between the secondary loop and the VOC-based inverters. Fig. 10 verify the reliable power sharing of the proposed control strategy under failure in the communication links at $t \geq 15$ s.

5. Experimental results

Experiments using two identical VOC-based single-phase inverters operated in the islanded mode verify the proposed control scheme. The values of the microgrid voltage and frequency, LCL filter, and secondary control parameters are identical to the parameters used for simulation, listed in Table 1. This necessitates a re-calculation of the VOC control

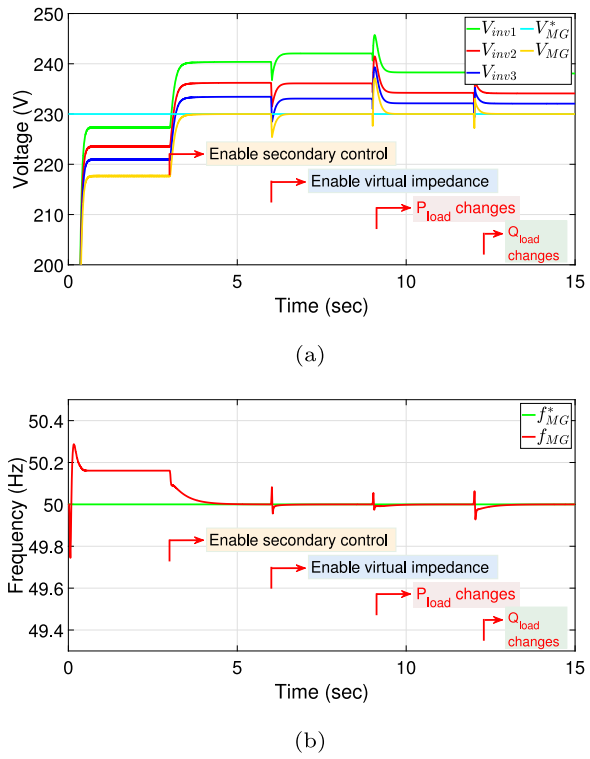

Fig. 9. Regulation of the microgrid:(a) voltages, (b) frequency.

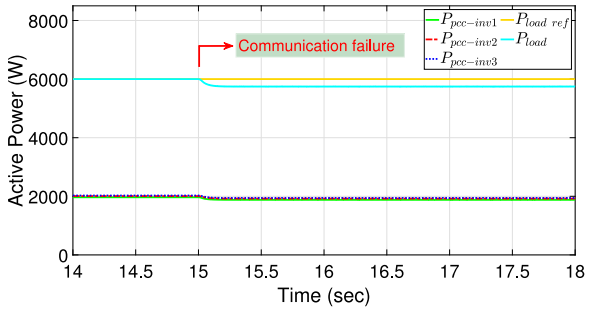

Fig. 10. Active power waveforms under communication failure.

parameters for the experiment as the inverters power rating is 2 kW in the lab. Additionally, the impedance of feeders 1 was set to $Z_{f1} = 1.3 + 0.5 \times 10^{-3}s$ and the impedance of feeders 2 varied between Z_{f1} and $0.5Z_{f1}$. The control algorithms of Inverter 1, 2 and the secondary control were implemented using TMS320F28379D ControlCARDs from Texas Instruments. Fig. 11 is a photograph of the experimental setup used.

The presented experimental results verified initially the effects of feeder impedances on power sharing accuracy. Then, the performance of the proposed virtual impedance technique to achieve power sharing, the online estimation of feeder impedances, and the proposed secondary control were validated as presented below.

Fig. 12(a) and Fig. 12(b) show the output current waveforms of the two identical VOC-based inverters under identical and nonidentical feeder impedances, respectively. The injected currents by Inverter 1 and 2 are identical in phase and magnitude only for the case of equal feeder impedances. Otherwise, Inverter 1 supplies less current for the case of $Z_{f2} = 0.5Z_{f1}$, according to the theoretical analysis shown in (6).

Fig. 13(a) and Fig. 13(b) verify the performance of the proposed virtual impedance for VOC-based inverters. The results were obtained where the impedances of feeders 1 and 2 were set to $Z_{f1} = 1.3 + 0.5 \times 10^{-3}s$ and $Z_{f2} = 0.65 + 0.25 \times 10^{-3}s$, respectively. It is evident that both VOC-based inverters share the load current unequally due to the unequal impedances of their feeders; see Fig. 13. However, these errors were regulated to zero after enabling the proposed virtual impedance for Inverter 2, which was calculated as presented in (10) where $Z_{v2} = Z_{f1} - Z_{f2}$.

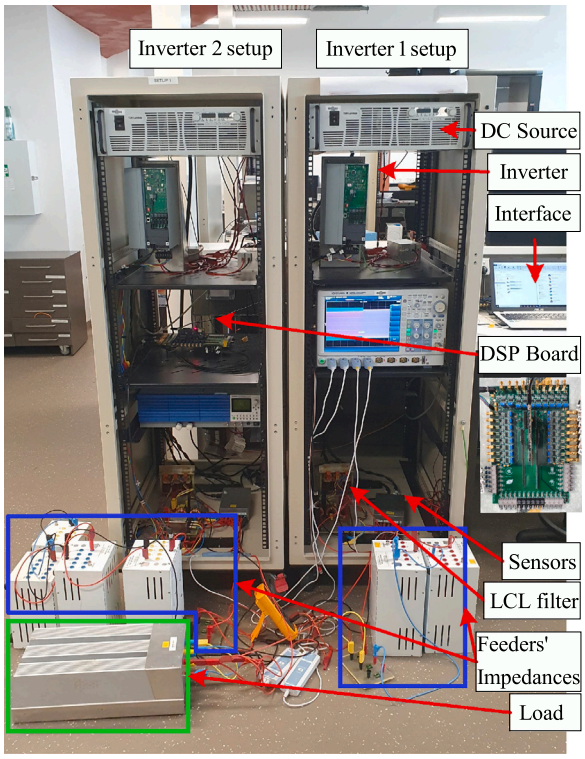

Fig. 11. The laboratory prototype consisting of two identical VOC-based inverters with an output LCL filter. The inverters are connected to a common load through respective RL line impedances.

Fig. 14 shows the load active power sharing by each inverter, where $R_{Load} = 32.85\ \Omega$. It can be observed that accurate sharing of the real power is achieved only after enabling the proposed control. Fig. 14 shows that the circulating reactive current between two inverters is suppressed almost to zero.

Fig. 15 validates the accurate realtime impedance estimation of feeder 1 by Inverter 1. For example, the estimated resistance is $\hat{R}_{f1}$= 1.35 Ω where its actual value is R_{f1}= 1.3 Ω. Similarly, the estimated inductance is $\hat{L}_{f1}$= 0.495 mH where its actual value is L_{f1}= 0.5 mH.

Figs. 16 to 18 show performance before and after enabling the proposed secondary control. Fig. 16 shows the voltage and currents waveforms of the microgrid load. Initially, the microgrid voltage was found to be equal to 202 V under the primary VOC control. This voltage drop is due to the feeder impedance (R_{f1}&L_{f1}), LCL filter impedance, and the dead-time of the VOC-based inverter. Then, the voltage is restored to its nominal value 230 V using the proposed secondary control loop. It can be seen from Fig. 16 that enabling the secondary control at 10 s (2 sec/div) is featured with fast transition capability, where there is now overshoot and it takes around 0.5 s to converge.

Fig. 17 shows the adaptive tuning of the VOC parameters k_v and L given by (7) and (8), respectively. Prior to enabling the secondary control, these parameters were set to their designed values at 253 V and 54.4 uH. Then, these values were adaptively tuned to 287.5 V and 54.5 uH, after enabling the secondary control to restore the microgrid nominal voltage and frequency.

Fig. 18 compares the load active power with its desired reference $P_{load\ ref}$ = 1610 W. Initially, the delivered power to the load was 1257 W, which is less than the desired value due to voltage drops. Then,

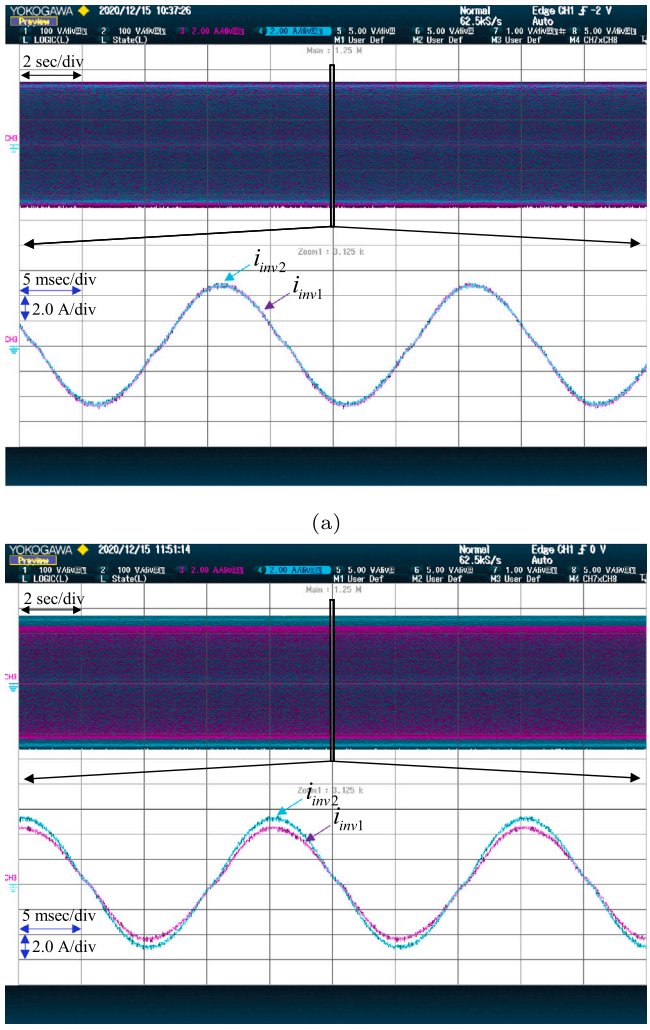

Fig. 12. Output current of the two identical VOC-based inverters with: (a) identical feeder impedances ($Z_{f2} = Z_{f1}$), (b) non-identical feeder impedances ($Z_{f2} = 0.5Z_{f1}$).

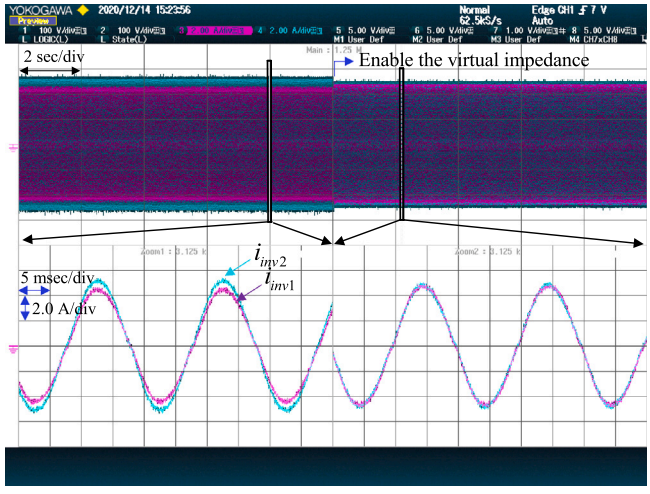

Fig. 13. Output current of Inverter 1 and Inverter 2 with non-identical feeder impedances ($Z_{f2} = 0.5Z_{f1}$) before and after enabling the proposed virtual impedance.

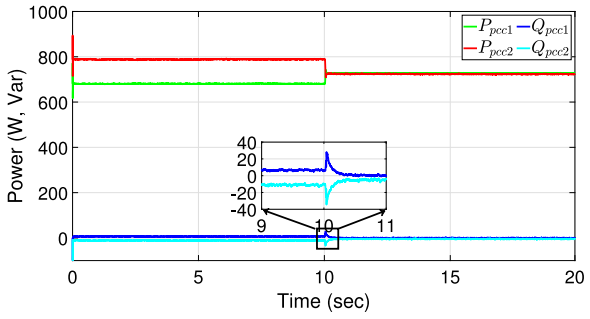

Fig. 14. Power sharing of the resistive load between two identical VOC-based inverters for $Z_{f2} = 0.5Z_{f1}$ before and after enabling the proposed virtual impedance. Also, small amount of reactive power are being circulated between the two inverters.

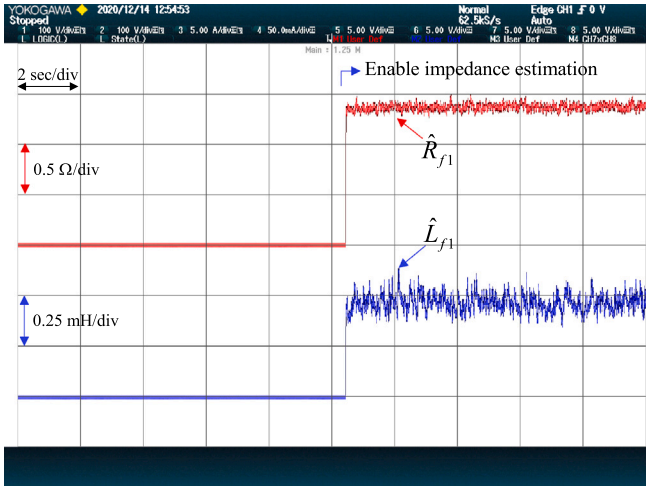

Fig. 15. Online estimation of resistance and inductance of feeder 1 by Inverter 1.

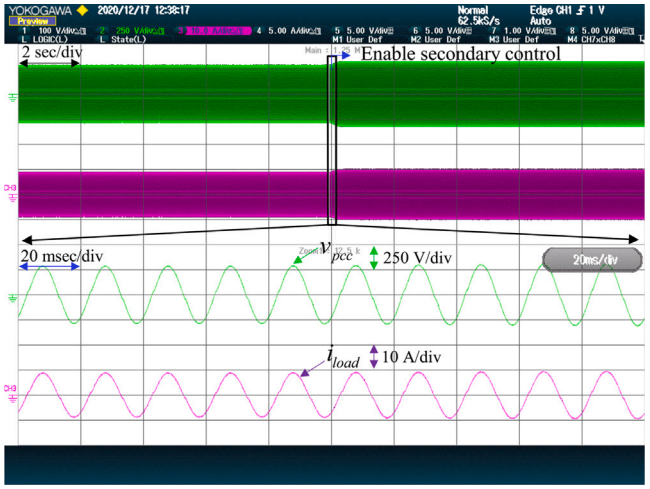

Fig. 16. Seamless transition after enabling the proposed secondary control loop: Voltage and current waveforms.

the supplied power to the load was regulated to its desired reference after enabling the proposed secondary control loop.

A related concern to point out is the microgrid architecture considered in this paper in which inverters are supplying a central load; see Fig. 3. The authors chose this architecture of the microgrid as it is the most commonly used in the literature to evaluate the accuracy of

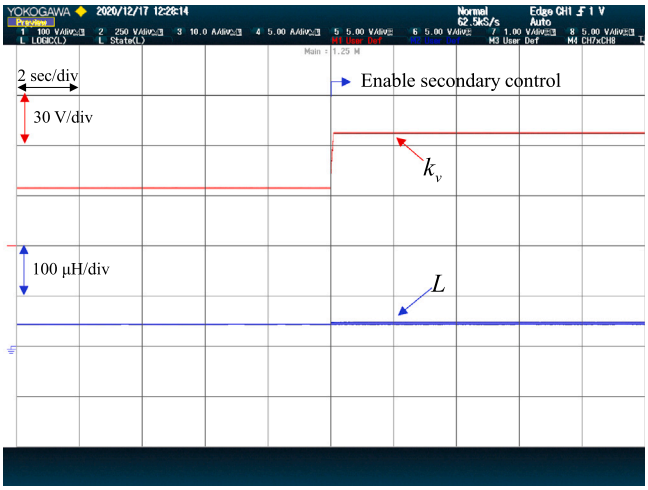

Fig. 17. Adaptive tuning of the VOC parameters, k_v and L after enabling the proposed secondary control loop.

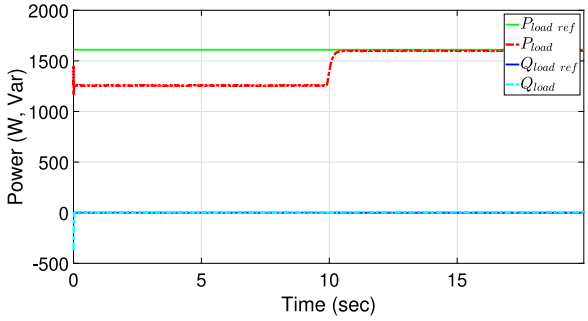

Fig. 18. Desired and supplied power to the microgrid load before and after enabling the proposed secondary control loop.

power sharing and performance of secondary control in inverter-based microgrids [9,11]. Future research can consider other types such mesh type AC microgrid architecture.

6. Conclusion

In this article, a new control approach for VOC-based islanded AC microgrids was proposed to restore the microgrid frequency and voltage and to improve the power sharing among the inverters. The proposed control consists of three main parts, namely: secondary control loop, an optimal tuning approach for virtual complex impedances, and online estimation technique of feeder impedances. First, in order to allow the restoration of the frequency and voltage, a secondary control loop based on the adaptive tuning of the VOC inductance and VOC voltage-scaling factor is proposed. Hence, fast dynamic response to the microgrid transients was accomplished. Then, to achieve accurate active and reactive power sharing among VOC-based inverters despite the existing impedance mismatch of the interfacing feeders, an optimal tuning approach of virtual complex impedance for each inverter is proposed. The tuning procedure of the virtual impedance based on the online estimation of feeder impedances was elaborated in detail. Simulation results, using MATLAB Simulink, of a single-phase islanded AC microgrids consisting of three VOC-based inverters are presented to test and validate the performance of the proposed control strategy. Then, the analysis is experimentally validated with two VOC-based inverters rated at 2 kW.

CRediT authorship contribution statement

Nabil Mohammed: Conceptualization, Methodology, Software, Validation, Formal analysis, Writing – original draft, Investigation, Visualization. **Muhammad Ali:** Validation, Formal analysis, Writing – review & editing. **Mihai Ciobotaru:** Methodology, Supervision, Writing – review & editing, Project administration. **John Fletcher:** Resources, Supervision, Writing – review & editing.

Declaration of competing interest

The authors declare that they have no known competing financial interests or personal relationships that could have appeared to influence the work reported in this paper.

Data availability

No data was used for the research described in the article.

References

[1] R. Secretariat, Renewables 2020 Global Status Report, Rep, REN12, Paris, 2020.
[2] A. Mohd, E. Ortjohann, D. Morton, O. Omari, Review of control techniques for inverters parallel operation, Electr. Power Syst. Res. 80 (12) (2010) 1477–1487.
[3] IRENA, Renewable energy statistics 2020 the international renewable energy agency, 2020, Abu Dhabi.
[4] A. Mohamed, O. Mohammed, Real-time energy management scheme for hybrid renewable energy systems in smart grid applications, Electr. Power Syst. Res. 96 (2013) 133–143.
[5] R.H. Lasseter, Microgrids, in: 2002 IEEE Power Engineering Society Winter Meeting. Conference Proceedings (Cat. No. 02CH37309), Vol. 1, 2002, pp. 305–308.
[6] N. Mohammed, M. Ciobotaru, Fast and accurate grid impedance estimation approach for stability analysis of grid-connected inverters, Electr. Power Syst. Res. 207 (1) (2022) 107831.
[7] G. Venkataramanan, C. Marnay, A larger role for microgrids, IEEE Power Energy Mag. 6 (3) (2008) 8–82.
[8] A. Chandra, G.K. Singh, V. Pant, Protection of AC microgrid integrated with renewable energy sources–a research review and future trends, Electr. Power Syst. Res. 193 (2021) 107036.
[9] Y. Han, H. Li, P. Shen, E.A.A. Coelho, J.M. Guerrero, Review of active and reactive power sharing strategies in hierarchical controlled microgrids, IEEE Trans. Power Electron. 32 (3) (2017) 2427–2451.
[10] M.C. Chandorkar, S. Member, M. Deepakraj, Control of parallel connected inverters in standalone AC supply systems, IEEE Trans. on Indus. Appl. 29 (1) (1993) 136–143.
[11] J.M. Guerrero, J.C. Vasquez, J. Matas, L.G. De Vicuña, M. Castilla, Hierarchical control of droop-controlled AC and DC microgrids a general approach toward standardization, IEEE Trans. on Indus. Electron. 58 (1) (2011) 158–172.
[12] J. He, Y.W. Li, Analysis, design, and implementation of virtual impedance for power electronics interfaced distributed generation, IEEE Trans. Ind. Appl. 47 (6) (2011) 2525–2538.
[13] J. Matas, M. Castilla, L. Garc, J. Miret, J.C. Vasquez, Virtual impedance loop for droop-controlled single-phase parallel inverters using a second-order general-integrator scheme, IEEE Trans. Power Electron. 25 (12) (2010) 2993–3002.
[14] J.M. Guerrero, L.G. De Vicuña, J. Matas, M. Castilla, Output impedance design of parallel-connected UPS inverters with wireless load-sharing control, IEEE Trans. on Indus. Electron. 52 (4) (2005) 1126–1135.
[15] J.M. Guerrero, J. Matas, L.G. De Vicuña, M. Castilla, J. Miret, Decentralized control for parallel operation of distributed generation inverters using resistive output impedance, IEEE Trans. on Indus. Electron. 54 (2) (2007) 994–1004.
[16] A. Micallef, M. Apap, C. Spiteri-Staines, J.M. Guerrero, J.C. Vasquez, Reactive power sharing and voltage harmonic distortion compensation of droop controlled single phase islanded microgrids, IEEE Trans. Smart Grid 5 (3) (2014) 1149–1158.
[17] C.N. Rowe, T.J. Summers, R.E. Betz, T.G. Moore, C.D. Townsend, Implementing the virtual output impedance concept in a three phase system utilising cascaded PI controllers in the dq rotating reference frame for microgrid inverter control, in: 15th Eur. Conf. Power Electron. Appl., 2013, pp. 1–10.
[18] H. Mahmood, S. Member, D. Michaelson, J. Jiang, S. Member, Accurate reactive power sharing in an islanded microgrid using adaptive virtual impedances, IEEE Trans. on Power Electron. 30 (3) (2015) 1605–1617.
[19] N. Mohammed, M. Ciobotaru, An accurate reactive power sharing strategy for an islanded microgrid based on online feeder impedance estimation, in: IECON 2020 the 46th Annual Conference of the IEEE Industrial Electronics Society, Singapore, Singapore, 2020, pp. 2525–2530.

[20] B.B. Johnson, S.V. Dhople, A.O. Hamadeh, P.T. Krein, Synchronization of parallel single-phase inverters with virtual oscillator control, IEEE Trans. Power Electron. 29 (11) (2014) 6124–6138.
[21] B. Johnson, M. Rodriguez, M. Sinha, S. Dhople, Comparison of virtual oscillator and droop control, in: 2017 IEEE 18th Work. Control Model. Power Electron. COMPEL 2017, 2017.
[22] M. Sinha, F. Dorfler, B.B. Johnson, S.V. Dhople, Uncovering droop control laws embedded within the nonlinear dynamics of Van der Pol oscillators, IEEE Trans. Control Netw. Syst. 4 (2) (2017) 347–358.
[23] B.B. Johnson, M. Sinha, N.G. Ainsworth, F. Dörfler, S.V. Dhople, Synthesizing virtual oscillators to control islanded inverters, IEEE Trans. Power Electron. 31 (8) (2016) 6002–6015.
[24] B.B. Johnson, S.V. Dhople, J.L. Cale, A.O. Hamadeh, P.T. Krein, Oscillator-based inverter control for islanded three-phase microgrids, IEEE J. Photovolt. 4 (1) (2014) 387–395.
[25] H. Yu, M.A. Awal, H. Tu, Y. Du, S. Lukic, I. Husain, A virtual impedance scheme for voltage harmonics suppression in virtual oscillator controlled islanded microgrids, in: 2020 IEEE Applied Power Electronics Conference and Exposition, APEC, New Orleans, LA, USA, 2020, pp. 609–615.
[26] M.A. Awal, H. Yu, I. Husain, W. Yu, S.M. Lukic, Selective harmonic current rejection for virtual oscillator controlled grid-forming voltage source converters, IEEE Trans. Power Electron. 35 (8) (2020) 8805–8818.
[27] M. Colombino, D. Groß, J.S. Brouillon, F. Dörfler, Global phase and magnitude synchronization of coupled oscillators with application to the control of grid-forming power inverters, IEEE Trans. Automat. Control 64 (11) (2019) 4496–4511, http://dx.doi.org/10.1109/TAC.2019.2898549.
[28] G.S. Seo, M. Colombino, I. Subotic, B. Johnson, D. Groß, F. Dörfler, Dispatchable virtual oscillator control for decentralized inverter-dominated power systems: Analysis and experiments, 2018, pp. 561–566, arXiv.
[29] D. Raisz, T.T. Thai, A. Monti, Power control of virtual oscillator controlled inverters in grid-connected mode, IEEE Trans. Power Electron. 34 (6) (2019) 5916–5926.
[30] M.A. Awal, H. Yu, H. Tu, S.M. Lukic, I. Husain, Hierarchical control for virtual oscillator based grid-connected and islanded microgrids, IEEE Trans. Power Electron. 35 (1) (2020) 988–1001.
[31] M. Ali, H.I. Nurdin, J. Fletcher, Dispatchable Virtual Oscillator Control for Single-Phase Islanded Inverters: Analysis and Experiments, in: IEEE Transactions on Industrial Electronics.
[32] S. Cobreces, E.J. Bueno, D. Pizarro, F.J. Rodriguez, F. Huerta, S. Member, Grid impedance monitoring system for distributed power generation electronic interfaces, IEEE Trans. on Instrum. and Measur. 58 (9) (2009) 3112–3121.